Surface-induced orientational order in stretched nanoscale-sized polymer dispersed liquid-crystal droplets

Ichiro Amimori,[1] James N. Eakin,[1] Jun Qi,[2] Gregor Skačej,[3] Slobodan Žumer,[3] and Gregory P. Crawford[1,2]
[1]*Division of Engineering, Brown University, Providence, Rhode Island 02912, USA*
[2]*Department of Physics, Brown University, Providence, Rhode Island 02912, USA*
[3]*Department of Physics, University of Ljubljana, Jadranska 19, SI-1000 Ljubljana, Slovenia*
(Received 3 September 2004; published 17 March 2005)

We investigate orientational ordering in stretched polymer-dispersed liquid-crystal (PDLC) droplets using deuterium nuclear magnetic resonance, in the nematic and isotropic phases. In the latter case, we estimate the surface order parameter S_0 and the thickness of the interfacial layer from the temperature-independent surface ordering model for an elliptical cavity with a varying aspect ratio. A simple phenomenological model well describes the quadrupole splitting frequency of NMR spectra in the isotropic phase. The strain dependence of S_0 suggests that stretching-induced changes in the orientation of polymer chains in the PDLC matrix noticeably affect liquid-crystal surface anchoring. Experimental results are supported by simulated NMR spectra obtained as output from Monte Carlo simulations of paranematic ordering in ellipsoidal droplets based on the Lebwohl-Lasher lattice model.

DOI: 10.1103/PhysRevE.71.031702 PACS number(s): 61.30.Pq, 61.30.Cz, 64.70.Md

I. INTRODUCTION

A liquid crystal in physical contact with a solid substrate is partially ordered even above the nematic-isotropic transition temperature. This phenomenon can be treated as orientational wetting of the substrate by the nematic phase at a temperature where the isotropic phase is stable in the bulk [1,2]. On approaching the nematic-isotropic (NI) transition temperature (T_{NI}) from above, the thickness of the ordered nematic surface layer assumes either a finite or infinite limiting value, which corresponds to partial or complete orientational wetting regime. To classify the wetting regime as either partial or complete, the adsorption parameter $\Gamma = \int_0^\infty S(z)dz$ is used, where z is the distance from the order-inducing surface and $S(z)$ the scalar orientational order parameter [3]. Neglecting biaxiality, the surface-induced ordering in the isotropic phase is well described by $S(z)$ and the preferred molecular direction $\mathbf{n}(\mathbf{r})$ in the surface layer. If Γ diverges as T_{NI} is approached, orientational wetting is known as complete; if Γ remains finite, it is said to be partial. The nature of the wetting regime is strongly correlated to the interaction strength between the liquid crystal and the orienting solid surface, and therefore depends on the magnitude of the surface-induced order parameter in the interfacial layer [4]. If the value of the surface order parameter S_0 exceeds a threshold order parameter S_c, then wetting is complete, while below S_c wetting is only partial. Within the Landau–de Gennes framework, the threshold value is equal to the bulk nematic order parameter at T_{NI} [1,2].

The pioneering work of Miyano demonstrated that the surface-induced order parameter could be accessed with pretransitional birefringence measurements [5]. Further experimental efforts include second-harmonic generation [6], field-induced twist [7], and evanescent-wave ellipsometry [8]. Over a decade ago, it was found by Crawford and coworkers that liquid crystals confined to Nuclepore cavities could be effectively probed with deuterium nuclear magnetic resonance (^{2}H-NMR) [9]. Since the surface-to-volume ratio in these confined systems was large and the orientation of the liquid crystal in the Nuclepore cavities was uniform with respect to the static magnetic NMR field, a small but measurable quadrupole splitting was measured above the T_{NI}. In fact, it was measurable to temperatures deep in the isotropic phase ($T - T_{NI} \sim 20$ K). This early study proved the validity of the ^{2}H-NMR technique in surface-induced order studies and showed that ^{2}H-NMR was capable of measuring S_0, the interfacial layer thickness l_0, and the molecular exchange rate between the ordered surface layer and the bulk. The ^{2}H-NMR technique was later used to study liquid crystals confined to alumina channels of Anopore membranes where anchoring transitions were observed and radically different values of S_0 were measured, depending on the surface alignment layer [3,4,10]. The work has recently been extended to smectic liquid crystals where NMR can measure the degree of smectic-nematic coupling [11] and pretransitional smectic layering phenomena [12]. In fact, the NMR technique has been applied to numerous confined liquid-crystal systems, including Vycor glass [13–15], silica aerogel [16], and Millipore filters [17]. Most recently, NMR has been used to probe layer order of mesogenic molecules deposited on the cavity walls of an Anopore membrane surface [18].

In contrast to intensive efforts devoted to liquid crystals confined to cylindrical and random geometries [19], surface parameters of polymer dispersed liquid crystals (PDLC's) have only been scarcely investigated in comparison. Golemme and co-workers used ^{2}H-NMR to study spherical liquid-crystal droplets [20]. In the pioneering publication on NMR to study PDLC's, they revealed that the weak first-order nematic-isotropic transition was replaced by a continuous evolution of order for sufficiently small droplets, a prediction made many years before by Sheng in planar samples [1] and later by Vilfan and co-workers in spherical droplets [21]. Studies of PDLC droplets have continued on far more than a decade after the seminal publication of Golemme and

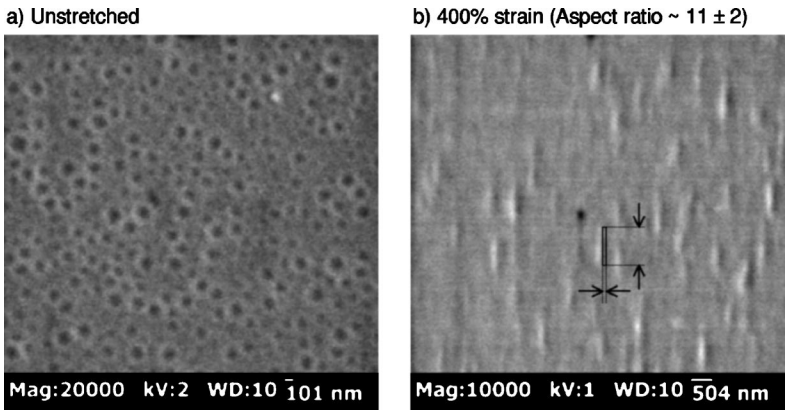

FIG. 1. SEM photographs of PDLC films: (a) before stretching, (b) 400% strain. The average initial diameter of undeformed droplets is (92 ± 16) nm. Arrows indicate the major and minor axes for one of the stretched droplets. The average axis lengths in the sample with 400% strain are estimated as (460 ± 80) nm and (41 ± 7) nm for the major and minor axes, respectively. The corresponding aspect ratio (measured from more than 100 droplets in several pictures) is 11 ± 2.

co-workers. NMR relaxometry was used to extract the value of S_0 from the transverse relaxation rate T_2^{-1} [22]. The ability to measure S_0 directly from the ^{2}H-NMR quadrupole splitting frequency in PDLC systems remains a challenge for two reasons: (1) the droplet director (average orientation of symmetry axis of liquid crystal droplet) differs from droplet to droplet with respect to the magnetic field direction and (2) there tends to be a much larger size distribution in PDLC's compared to the well-defined pores of Nuclepore and Anopore membranes [3,4,10].

On the other hand, with the continuous increase of computing power, as well as with the development of simulation techniques, strongly confined liquid-crystal systems are becoming increasingly accessible to computer simulation studies. In particular, a lot of effort has been invested into exploring nematic ordering inside PDLC droplets, where most of the analyses were based on the computationally simple Lebwohl-Lasher lattice model. Typically, Monte Carlo (MC) simulations were carried out for this model system [23]. The resulting numerical output can be expressed in terms of suitable order parameters or, even more conveniently, directly in terms of macroscopic experimental observables such as ^{2}H-NMR spectra. The methodology for calculating dynamic NMR spectra, capable of handling fluctuations of molecular long axes and translational diffusion, has been presented and tested for spherical PDLC droplets [24]. More recent MC studies of nematic ordering extend to elliptical droplets as well [25,26].

In this contribution we report on a PDLC system that gives a reasonable quadrupole splitting in the isotropic phase. After PDLC formation using the emulsification technique [27], the PDLC film is subjected to a high degree of uniaxial strain (as much as 400%) to create ellipsoidal droplets whose droplet director and cross section are nearly uniform [28]. These highly aligned droplet samples, currently being developed for light scattering polarizer applications [29], create an ideal system to be studied with ^{2}H-NMR. We present an experimental determination of the surface-induced order parameter S_0 directly obtained from the quadrupole splitting frequency measured above T_{NI}. The experimental work is complemented with quadrupole splitting data derived from MC simulations.

II. SAMPLE PREPARATION AND EXPERIMENTAL METHOD

PDLC films used in this study consisted of dispersions of deuterated 4′-pentyl-4-cyanobiphenyl (5CB-αd_2) and polyvinyl alcohol PVA205 (molecular weight: 25 000, degree of hydrolysis: 88%, Kuraray Co., Ltd.), which is a water-soluble polymer. A 20 wt % aqueous solution of PVA was mixed with the liquid crystal and then dispersed in water [30]. We used an ultrasonic processor (CPX-400, 400 W, 20 kHz, Cole-Parmer Instrument Co.) at 40% output with 1/8-in. microtip to emulsify the liquid crystal into the PVA aqueous solution. The emulsion was then coated on a smooth polyethylene terephthalate (PET) substrate using a Meyer Bar and processed under ambient conditions. After the water evaporated, the polymer film was carefully released (peeled) from the substrate. The film thickness was approximately (16 ± 4) μm and the concentration of liquid crystal in the film was 25 wt %. The film was stretched to the desired strain (5%, 20%, 100%, and 400%), cut into strips 20 mm $\times$6 mm, stacked such that the thickness was more than 50 μm, and carefully inserted into a NMR tube.

Figure 1(a) shows scanning electron microscope (SEM) images of a PDLC film before stretching when droplets are approximately spherical. After stretching, the droplets become elongated, with their major axes along the stretch direction, as shown in Fig. 1(b) [31]. The stretching is accompanied by an alignment of the nematic director parallel to the stretch direction within each droplet, which has been proven using optical polarization measurements [26,28,29]. The average diameter in Fig. 1 was measured to be (92 ± 16) nm. Assuming that the liquid-crystal droplet was incompressible and its initial shape spherical, the minor semiaxis R_0 after stretching is approximated by

$$R_0 \sim R_{ini}(1+\epsilon)^{-1/2}, \tag{1}$$

where R_{ini} is the initial radius $[(46\pm8)$ nm$]$ and ϵ is the strain. Note that even at zero strain the droplet shapes are not perfectly spherical, but are close to oblate spheroids with their minor axes perpendicular to the film plane [27]. Then, assuming Poisson ratio to be isotropic [32], Eq. (1) is still valid when we define R_{ini} as the initial length of one of the principal axes. Figure 1(b) shows the droplets after they have been subjected to 400% strain.

The stretched PDLC film was stacked in the NMR tube such that the stretched axis of the film was parallel to the magnetic field. The NMR experiments were performed on a solid-state spectrometer (AVANCE 300/Ultrashield, 300 MHz, 89 mm, Bruker BioSpin GmbH) with a 7.05-T magnetic field. A modified quadrupolar echo sequence

$(\pi/2)_x$-τ-$(\pi/2)_y$ was employed, where $\tau=100$ ms and the length of the $\pi/2$ pulse was 10 μs. The free-induction decay (FID) was averaged more than 10 000 times to achieve a reasonable signal-to-noise ratio. The temperature in the sample probe was controlled to within ±0.1 °C.

III. NMR TECHNIQUE

Deuterium nuclei have been used frequently as a NMR probe in studies of molecular structure and dynamics in liquid crystals. ^{2}H-NMR provides the orientational order at the molecular level via time-averaged quadrupole splitting frequency from selectively deuterated liquid-crystal molecules. In the absence of motional averaging, a deuterated molecule at position **r** within a droplet will yield a spectrum of two sharp lines separated by

$$\delta\nu(\mathbf{r}) = \frac{\delta\nu_B}{S_B} S(\mathbf{r}) \left[\frac{3}{2}\cos^2\theta_B(\mathbf{r}) - \frac{1}{2} \right], \tag{2}$$

where $\theta_B(\mathbf{r})$ is the angle between the local nematic director and the magnetic field, $S(\mathbf{r})$ the local order parameter, and $\delta\nu_B/S_B$ the ratio between the quadrupole splitting frequency and the order parameter of the bulk nematic. $\delta\nu_B/S_B$ for 5CB in the nematic phase is 87.5 kHz [10].

Our work focuses on uniaxially stretched PDLC's using 5CB-αd_2. In our case the magnetic coherence length $\xi_m = B^{-1}\sqrt{\mu_0 K/\Delta\chi}$ is $\xi_m \sim 1.1$ μm [33] for reported values of $\Delta\chi = 1.2\times10^{-7}$, the anisotropy of the diamagnetic susceptibility, $K = 6\times10^{-12}$ N, the elastic constant, and $\mu_0 = 4\pi \times 10^{-7}$ N/A^2, the permeability of free space. ξ_m is significantly larger than our droplet radii R so that the field has no appreciable aligning effect. Further, the characteristic length of diffusion in a NMR measurement is $d \sim \sqrt{D/\delta\nu}$. Here $D \sim 10^{-10}$ m^2/s is the diffusion constant and $\delta\nu$ a characteristic frequency in the NMR spectrum. Then, in the nematic phase one has $\delta\nu \sim \delta\nu_B = 52.1$ kHz, yielding $d \sim 44$ nm, while in the isotropic phase one obtains $\delta\nu \sim 500$ Hz and $d \sim 450$ nm. In our case, $d \gg R$ in the isotropic phase, therefore we can expect complete diffusional averaging.

IV. LIQUID-CRYSTAL ALIGNMENT IN THE NEMATIC PHASE

According to optical polarization measurements, liquid-crystal molecules confined within stretched PDLC droplets on average align parallel to the stretch direction [26,28,29]. This alignment was observed via a change in birefringence of the droplets and was not directly measured. In order to directly investigate the liquid-crystal alignment, we analyzed NMR spectra of stretched PDLC films in nematic phase. Figure 2 illustrates the coordinate system of the NMR samples. By orienting the NMR magnetic field parallel to X, Y, and Z, we can independently measure the liquid-crystal director distribution with respect to these three axes. We measured NMR spectra in the nematic phase at 298 K.

Figure 3 shows the NMR spectra of 5CB-αd_2 in an unstretched PDLC film [Figs. 3(a) and 3(b)] and in the bulk [Fig. 3(c)], as well as a schematic depiction of liquid-crystal alignment within droplets. Both NMR measurements where

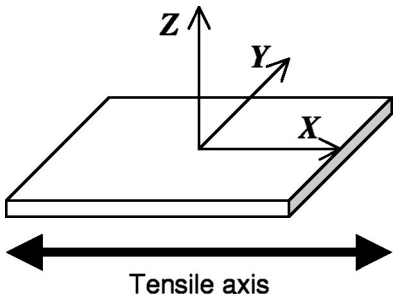

FIG. 2. The schematic diagram of the coordinate system of NMR measurement.

the magnetic field is in the X and Y directions (Fig. 2) are equivalent for geometrical reasons. From Eq. (2), the quadrupole splitting frequency at $\theta_B = 90°$ is one-half that of the bulk-aligned splitting. The quadrupole splitting frequency in the unstretched PDLC when the magnetic field is along Z axis [Fig. 3(a)] is nearly one-half that of the bulk [Fig. 3(c)], which indicates that liquid-crystal molecules align predominantly perpendicular to the Z axis in this composite. Moreover, Fig. 3(b) is similar to a Pake-type powder spectrum obtained from a two-dimensional random distribution of liquid-crystal molecules [34]. These results indicate that ordering in droplets is bipolar and that bipolar symmetry axes are randomly oriented in the XY plane. This is in agreement with the fact that the PDLC film collapses along the Z axis

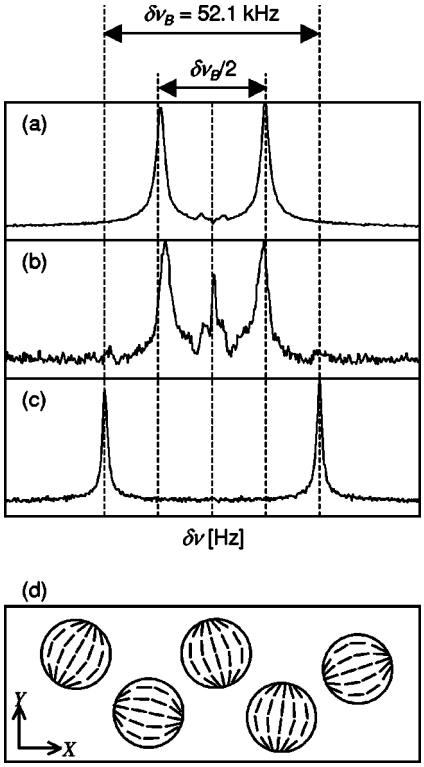

FIG. 3. The NMR spectra of 5CB-αd_2 in an unstretched PDLC film with (a) the magnetic field applied along the Z axis and (b) Y axis, and (c) in a bulk sample aligned parallel to the magnetic field. (d) Schematic depiction of droplet organization: bipolar axes not aligned.

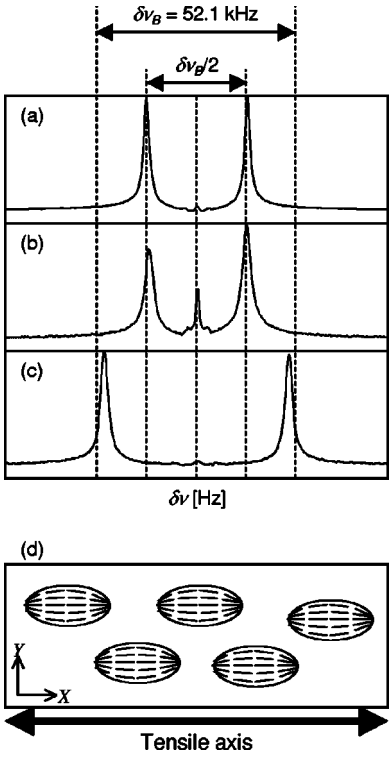

FIG. 4. The NMR spectra of 5CB-αd_2 in a 100% stretched PDLC film: (a) magnetic field along the Z axis, (b) magnetic field along the Y axis, (c) magnetic field along the X axis. (d) Schematic depiction of droplet organization: bipolar axes aligned.

during the evaporation process, and then the droplet shape becomes an oblate spheroid with the minor axis perpendicular to the film plane [27]. Such a film is schematically represented in Fig. 3(d). The reason why the quadrupole line-splitting frequency is slightly smaller than the expected bulk values is attributed to the curvature of the director field in the droplet [35].

Figure 4 shows the NMR spectra of 100% stretched PDLC film [Figs. 4(a), 4(b), and 4(c)] and the resulting liquid-crystal alignment [Fig. 4(d)]. When the magnetic field is directed along the Y (or Z) axis, the quadrupole splitting frequency approaches one-half of the bulk value, while for the magnetic field along the X axis the splitting is the almost the same as that of the bulk. Consequently, liquid-crystal molecules in PDLC are mostly aligned along the X axis. We have also investigated 5%, 20%, 100%, and 400% stretched PDLC films and compared them to the aligned bulk sample, as shown in Fig. 5. We found that liquid-crystal molecules are aligned in all samples, even for the 5% sample. These highly aligned systems enable us to extend our NMR study also to the isotropic phase, since the sample can be aligned such that the director is parallel to the magnetic field providing a maximum splitting.

V. SURFACE-INDUCED ORDER IN ISOTROPIC PHASE

Up to this part we have confirmed molecular alignment inside droplets in the nematic phase. This was essential to obtain reliable information on the effective aligning tendency

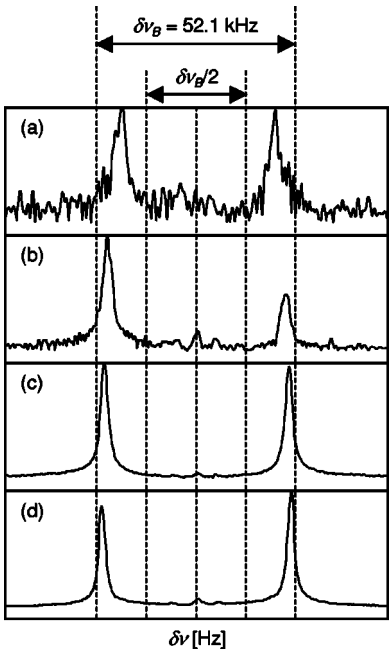

FIG. 5. The NMR spectra of 5CB-αd_2 in (a) 5%, (b) 20%, (c) 100%, and (d) 400% stretched PDLC films. The magnetic field is applied along the X axis.

of the polymer matrix that was shown to be of great importance in stretched PDLC systems [26,29]. In this section we study stretched PDLC films in the isotropic phase and show how to detect changes in the local aligning power of the confining matrix that determines the degree of surface-induced order. The same approach has already been successfully applied to nematics in cylindrical confinement [10] and will be adapted here to the elliptical geometry characterizing our PDLC systems. Note that both versions of the approach share the underlying basic physical phenomena.

First consider a one-dimensional case where the x axis represents the normal of a confining wall located at $x=0$. In the isotropic phase the degree of nematic order decays when moving away from the wall. This can be formally described by the Landau–de Gennes formalism for the nematic-isotropic transition giving a phenomenological expression for the free-energy density f [36,37]. In such a case f can be expanded in terms of a single order parameter $S(x)$ and is expressed as

$$f = f_0 + f_1[S(x)] + \frac{L}{2}[\nabla S(x)]^2 + g[S(x) - S_s]^2 \delta(x), \quad (3)$$

where S_s is the surface-imposed degree of order, while $g > 0$ and $L > 0$ are phenomenological constants. Moreover, f_0 is the S-independent part of the free energy density and $f_1[S(x)]$ is given by

$$f_1[S(x)] = \frac{a}{2}(T - T^*)S^2(x) - \frac{B}{3}S^3(x) + \frac{C}{4}S^4(x). \quad (4)$$

Here T denotes temperature, T^* the limit of supercooling, and $a > 0$, $B > 0$, and $C > 0$ are phenomenological constants. The final term in Eq. (3) is the surface contribution where g re-

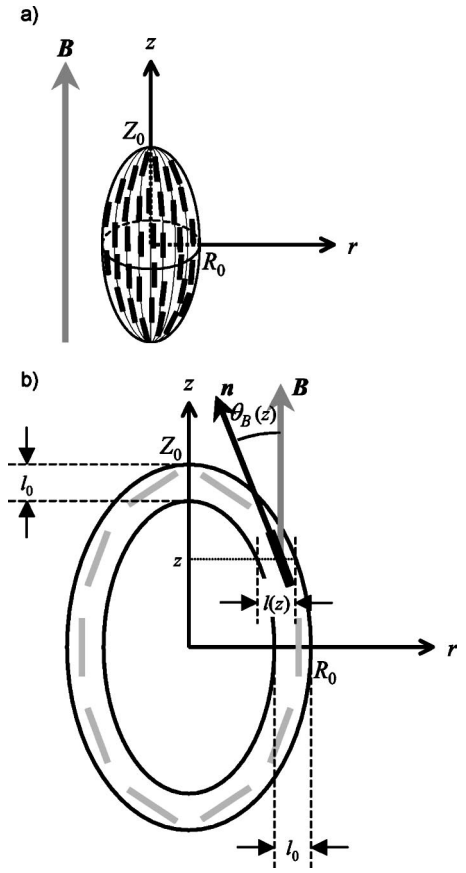

FIG. 6. Schematic diagram of the elliptical geometry: (a) cylindrical coordinate system for elliptical geometry, (b) surface molecule alignment with respect to the elliptical surface and the applied magnetic field.

flects the magnitude of the liquid-crystal–solid substrate interaction [3]. The total free energy is obtained by integrating Eq. (3) over the volume of the cavity:

$$F = \int_V \left(f_0 + f_1[S(x)] + \frac{L}{2}[\nabla S(x)]^2 \right) dV + \frac{1}{2} gA(S_0 - S_s)^2. \tag{5}$$

Here S_0 is the actual order parameter at the surface and A the surface area.

Assuming the degree of surface-induced order in the isotropic phase to be low, in Eq. (4) higher-order terms $S^3(x)$ and $S^4(x)$ can be neglected. Minimizing the total free energy, the order parameter as a function of x exhibits an exponential decay

$$S(x) = S_0 e^{-x/\xi}, \tag{6}$$

with ξ standing for the correlation length associated with nematic ordering. It is given by

$$\xi = \xi_0 \sqrt{\frac{T^*}{T - T^*}}, \tag{7}$$

where $\xi_0 \sim 0.65$ nm [38] and ξ diverges at T^* [36]. For 5CB, $T_{NI} - T^* = 2B^2/9aC \sim 1.1$ K.

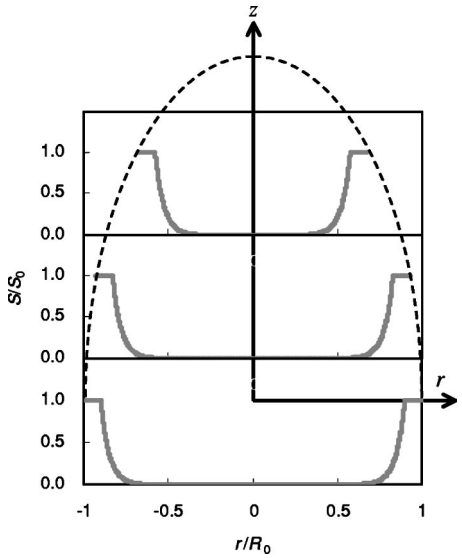

FIG. 7. The molecular orientational order parameter profile in an elliptical cavity at different z. The dashed line illustrates the surface of the elliptical cavity.

The actual degree of nematic order at the surface, S_0, can in principle exhibit a temperature dependence. Calculating the total free energy in a semi-infinite sample and minimizing it with respect to S_0 gives

$$S_0 = \frac{S_s}{1 + \sqrt{a(T - T^*)L}/2g}. \tag{8}$$

For $2g \gg \sqrt{a(T-T^*)L}$ (e.g., close to the nematic-isotropic transition) S_0 approaches S_s and is essentially temperature independent. On the contrary, if $2g \ll \sqrt{a(T-T^*)L}$, one has [10]

$$S_0 \approx \frac{S_{00}}{2\sqrt{T/T^* - 1}}, \tag{9}$$

where $S_{00} = 4gS_s/\sqrt{aT^*L}$ has been introduced. The two limits will be referred to as the "temperature-independent model" and the "temperature-dependent model" in this paper.

However, the above equations based on a continuum description sometimes do not adequately describe experimental results. An improved interfacial surface-layer model has been proposed and implemented in many systems [10]. The profile of the surface-induced nematic order is modified as

$$S(x) = \begin{cases} S_0, & 0 \leqslant x \leqslant l_0, \\ S_0 e^{-(x-l_0)/\xi}, & x > l_0, \end{cases} \tag{10}$$

where l_0 is the interfacial thickness of the surface layer (characterized by a constant degree of nematic order) and is approximately of the order of molecular dimensions.

A. Ellipsoidal droplet

The shape of stretched PDLC droplets can be represented as ellipsoidal, as suggested by the SEM image [Fig. 1(b)]. Figure 6 introduces the coordinate system: the z axis is taken along the long axis of the droplet (which coincides with the

bipolar axis of the nematic alignment) and r is the distance from the z axis. Here we discuss the case in which the NMR magnetic field is directed along z. The droplet center is chosen at $z=0$.

$$S(r,z)=\begin{cases} S_0, & R(z)\geqslant r\geqslant R(z)-l(z), \\ S_0 e^{-\{[R(z)-l(z)]-r\}/\xi(z)}, & R(z)-l(z)\geqslant r\geqslant 0. \end{cases} \tag{11}$$

Here $R(z)=R_0\sqrt{1-z^2/Z_0^2}$ is the radius of the slice centered at z, with R_0 and Z_0 denoting the length of the ellipsoid axes (see Fig. 6). Denoting with $\theta(z)$ the angle between the surface bipolar vector and the z axis, $l(z)=l_0/\cos\theta(z)$ and $\xi(z)=\xi/\cos\theta(z)$ define the thickness of the ordered interfacial layer, with

$$\cos\theta(z)=\sqrt{\frac{Z_0^2-z^2}{Z_0^2-z^2(1-\rho^{-2})}}. \tag{12}$$

(Here $\rho=Z_0/R_0$ is the aspect ratio of the ellipse.) Figure 7 shows $S(r,z)/S_0$ as a function of r/R_0 at different z: the ellipse composed of cylindrical slices with diameters $R(z)$.

The $S(r,z)$ order parameter profile can now be used to predict the quadrupole splitting in ^{2}H-NMR spectra. For tangential anchoring in an ellipsoid with the major axis parallel to the spectrometer magnetic field, the director will change its relative direction to the magnetic field parametrized by the angle $\theta_B(z)$, as shown in Fig. 6. In the case of strong anchoring it is $\theta_B(z)=\theta(z)$. Assuming complete diffusional averaging, the quadrupole splitting can be obtained as a spatial average of Eq. (2)—i.e.,

$$\langle\delta\nu(\mathbf{r})\rangle=\frac{\delta\nu_B}{S_B}\frac{\int_0^{Z_0}\int_0^{R(z)} rdrdzS(r,z)\left[\frac{3}{2}\cos^2\theta_B(z)-\frac{1}{2}\right]}{\int_0^{Z_0}\int_0^{R(z)} rdrdz}$$

$$=\frac{3S_0E(\rho)}{4R_0}\frac{\delta\nu_B}{S_B}(l_0+\xi), \tag{13}$$

where

$$E(\rho)=\frac{2\rho^2+1}{\rho(\rho^2-1)}+\frac{\rho(2\rho^2-5)}{(\rho^2-1)^{3/2}}\arctan(\sqrt{\rho^2-1}). \tag{14}$$

Above, $R(z)\gg\xi,l_0$ has been assumed, which fails in the very vicinity of droplet poles at $z=\pm Z_0$; however, the corresponding contribution to $\langle\delta\nu(\mathbf{r})\rangle$ is negligible. At $\rho=1$ where the sample is unstretched, $E(\rho=1)=2$. As ρ increases, $E(\rho)$ increases monotonically and saturates at $E(\rho\to\infty)=\pi$. Therefore, at large ρ, Eq. (13) reduces to $\langle\delta\nu(\mathbf{r})\rangle=3\pi S_0\delta\nu_B(l_0+\xi)/4R_0S_B$. Here ρ can be determined experimentally or is deduced from Eq. (1) as

Splitting the ellipsoid into slices along z and following the approach used for cylindrical cavities presented in Ref. [10], one can adapt the result given in Eq. (10) and approximately write

$$\rho=(1+\epsilon)^{3/2}. \tag{15}$$

Finally, by combining Eqs. (7), (9), and (13) we obtain the two expressions for the average splitting:

$$\langle\delta\nu\rangle=\frac{3E(\rho)}{8R_0}\frac{\delta\nu_B}{S_B}S_{00}\left[\frac{\xi_0T^*}{T-T^*}+\frac{l_0\sqrt{T^*}}{(T-T^*)^{1/2}}\right], \tag{16}$$

$$\langle\delta\nu\rangle=\frac{3E(\rho)}{4R_0}\frac{\delta\nu_B}{S_B}S_0\left[\frac{\xi_0\sqrt{T^*}}{(T-T^*)^{1/2}}+l_0\right]. \tag{17}$$

Equation (16) represents the limit with the temperature-dependent S_0, while Eq. (17) is the limit with the temperature-independent S_0 obtained for large g. By fitting the experimental data $\langle\delta\nu\rangle$, we can estimate the parameters l_0, S_0, and S_{00} that characterize the ordering in the interfacial layer. T^* is a fitting parameter as well [10].

B. Surface-induced orientational order of stretched PDLC's in the isotropic phase

We will now check which of the above limits (temperature-dependent or constant S_0) is suitable for our

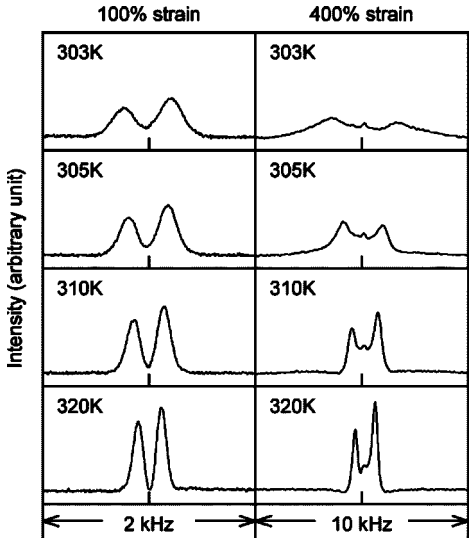

FIG. 8. ^{2}H-NMR spectra for 5CB-αd_2 of 100% and 400% stretched PDLC films in the isotropic phase. The magnetic field is parallel to the tensile axis (X axis).

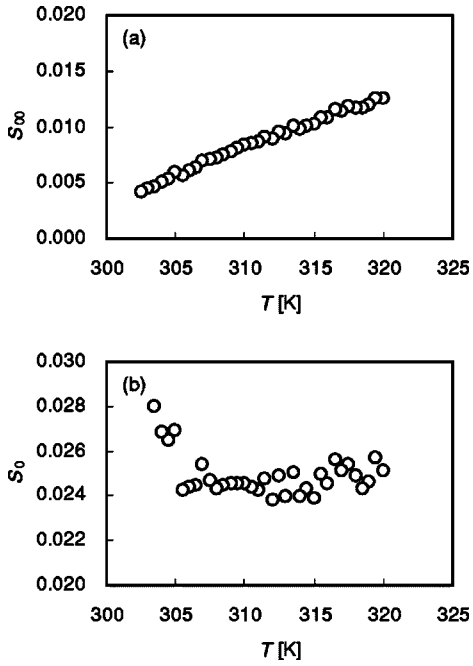

FIG. 9. Temperature dependence of the degree of surface-induced nematic order: (a) S_{00} calculated from Eq. (16) and (b) S_0 calculated from Eq. (17), with $\xi_0=0.65$ nm, $T^*=300.9$ K, and $l_0=1.0$ nm, both for 400% strain.

analysis. Figure 8 shows the NMR spectra of 100% and 400% stretched PDLC films in isotropic phase as a function of temperature. The quadrupolar line splitting decreases as the temperature increases in all samples. In terms of strain, the quadrupole line splitting increases as the strain increases. From Eq. (15), a 400% stretched sample gives $\rho \sim 11$, which is large enough to put $E(\rho)=\pi$. Figure 9 shows the temperature dependence of S_{00} calculated from Eq. (16), as well as S_0 calculated from Eq. (17), where $\xi_0=0.65$ nm, $l_0=1.0$ nm, and $T^*=300.9$ K (obtained from bulk $T_{NI}=302$ K), to roughly estimate the temperature dependence of S_{00} and S_0 [10]. According to the assumption, both S_{00} and S_0 should be

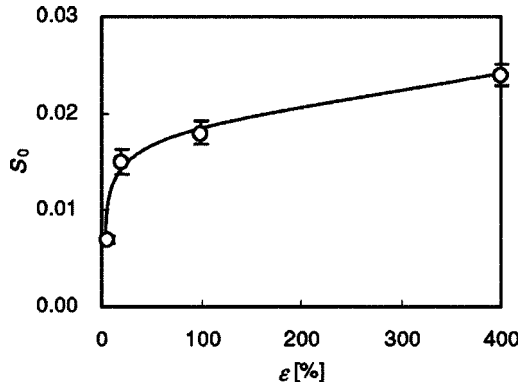

FIG. 11. Strain dependence of S_0.

constant, but S_{00} increases with temperature. Since this result indicates that the temperature-dependent model is not valid for the stretched PDLC, we employed the temperature-independent model to analyze the surface order parameter in our particular system.

Figure 10 shows the temperature dependence of the quadrupole splitting frequency for 5CB-αd_2 in 5%, 20%, 100%, and 400% stretched PDLC films. The solid line in Fig. 10 is the best fit result for Eq. (17), and values of S_0 and l_0 calculated from the best fit are shown as well. ρ is obtained from Eq. (15) and then $E(\rho)$ is calculated from Eq. (14). R_0 is estimated from Eq. (1) with $R_{ini}=46$ nm based on our SEM observation. ξ_0 used is 0.65 nm. The resulting values of $S_0=0.007-0.024$ are close to the reported value of $S_0=0.021$ for 5CB in Anopore membranes with untreated surface, and the value of $l_0=(0.00-1.61)$ nm is also close to the reported value of $l_0=(1.04-1.93)$ nm for 5CB in Anopore membranes with various surface treatments [10]. Figure 11 shows the strain dependence of S_0. S_0 increases quickly from 0% to 50% strain and then saturates during stretching. This behavior suggests that the alignment of liquid-crystal molecules within droplets confined in a PVA polymer matrix is influenced by polymer chain alignment induced by uniaxial stretching [29]. According to the optomechanical analysis of

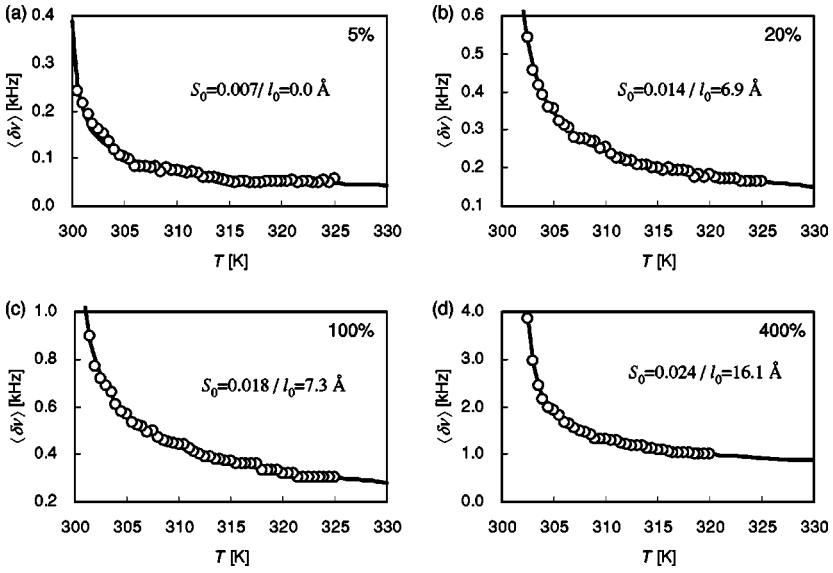

FIG. 10. Temperature dependence of the quadrupole splitting frequency $\langle \delta\nu \rangle$ of 5%, 20%, 100% and 400% stretched PDLC in isotropic phase. Solid curves are the best fits for the temperature-independent model given by Eq. (17).

TABLE I. Summary of interfacial parameters for 5CB-αd_2 confined to elliptical droplets of stretched PDLC films.

ϵ [%]	S_0 [−]	l_0 [nm]	T^* [K]	$\frac{1}{2}\sqrt{a(T_{NI}-T^*)L}$ [$\times 10^{-4}$(J/m^2)]
5	0.0070±0.0004	0.00±0.00	301.36±0.25	5.99±1.19
20	0.015±0.001	0.69±0.03	300.71±0.25	8.50±0.83
100	0.018±0.001	0.72±0.08	300.70±0.25	8.54±0.83
400	0.024±0.001	1.61±0.08	301.67±0.25	4.30±1.79

the PDLC film, the elastic region where polymer chains have not disentangled appears between 0% and 7% strain, the disentanglement region where polymer chains are disentangling appears from 7% to 35% strain, and the sliding regime where polymer chains are fully disentangled appears above 35% strain. NMR results indicate that the polymer chain orientation does influence liquid-crystal molecules on the polymer surface.

From the validity condition for the temperature-independent model one can estimate the two parameters that characterize the nematic coupling with the polymer substrate, g and S_s. For the coupling strength g one can derive the lower limit—i.e., $g \gg \frac{1}{2}\sqrt{a(T-T^*)L} \gtrsim \frac{1}{2}\sqrt{a(T_{NI}-T^*)L}$—while for the surface-imposed degree of order S_s one has $S_s \approx S_0$. S_0, l_0, T^*, and the limiting g are summarized in Table I, assuming $T_{NI}=302$ K (bulk value), $L=1.7\times10^{-11}$ J/m, and $a=0.1319\times10^6$ J/m^3 K [38]. The fact that the fitted T^* values vary from sample to sample is believed to largely originate in the presence of impurities left over from the polymerization process. This and other effects (especially confinement) result in a suppression of the NI transition in comparison with a bulk system [27].

VI. MONTE CARLO SIMULATIONS

In this section we briefly describe Monte Carlo simulations of paranematic ordering in nematic droplets for a strained PDLC sample, where the deformation of the polymer matrix is assumed to result in an ellipsoidal droplet shape. There are several reasons for performing MC simulations in this case: (i) they avoid the simplifying assumptions used in the phenomenological part of the study, (ii) they provide direct insight into molecular ordering mechanisms, and (iii) they can be used to predict dynamic NMR spectra. Our simulations are based on the Lebwohl-Lasher (LL) lattice model [39] in which uniaxial nematic molecules or close-packed molecular clusters are represented by unit vectors ("particles") $\mathbf{u}_i$. The particles are fixed onto sites of a cubic lattice whose lattice spacing p is estimated as 1 nm $\lesssim p \lesssim$ 5 nm assuming that the molecular clusters contain up to 10^2 nematic molecules [23]. The standard N-particle LL Hamiltonian reads [23,39]

$$U_N = -J\sum_{\langle i<j\rangle} P_2(\mathbf{u}_i\cdot\mathbf{u}_j), \tag{18}$$

where $P_2(x)\equiv\frac{1}{2}(3x^2-1)$, $J>0$ is a constant, and the sum runs over nearest-neighbor particles only. The Hamiltonian (18) promotes parallel alignment, which facilitates the formation of the nematic phase. The boundary conditions are determined by a layer of "ghost" particles whose orientations are fixed during the simulation. In our case we choose perfect bipolar boundary conditions—appropriately rescaled for strained droplets—in agreement with experimental observations reported in Sec. IV. Moreover, the bipolar and tensile axes are chosen to coincide. The interaction strength J is taken equal for nematic-nematic and nematic-ghost interactions, which implies strong anchoring, as already assumed in Sec. V A.

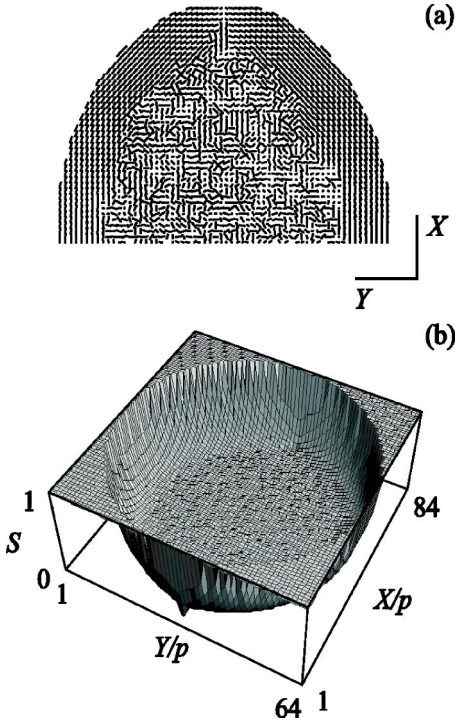

FIG. 12. Bipolar droplet with 20% strain at $\mathcal{T}=1.20$: simulated director field (a) and nematic order parameter map (b) (half and whole XY cross section through the droplet center, respectively), calculated by diagonalizing the MC-time-averaged local ordering matrix $\mathbf{Q}(i)=\frac{1}{2}(3\langle\mathbf{u}_i\otimes\mathbf{u}_i\rangle-I)$ [40].

Because of strong confinement translational diffusion cannot be ignored in the simulation of the NMR experiment (see the estimate in Sec. III). The calculation of ^{2}H-NMR spectra from the MC simulation output hence follows the procedure described in Ref. [24], which is applicable also in presence of significant molecular motion. First, the FID signal is generated in a reference frame rotating with Larmor frequency, i.e.,

$$G(t) = \left\langle \exp\left[i\int_0^t \Omega_Q^j(t')dt' \right] \right\rangle_j, \tag{19}$$

and is then Fourier transformed to yield the spectrum $I(\delta\nu)=\int\exp(i2\pi\delta\nu t)G(t)dt$. In Eq. (19) one has $\Omega_Q^j(t)=\pm\pi\delta\nu_B S_B^{-1}[3(\mathbf{u}_j\cdot\mathbf{b})^2-1]$, where $\mathbf{u}_j=\mathbf{u}_j(t)$ stands for the "instantaneous" orientation of the jth particle, $\mathbf{b}$ represents a unit vector along the magnetic field of the NMR spectrometer, and $\langle\cdots\rangle_j$ denotes an ensemble average over all particles

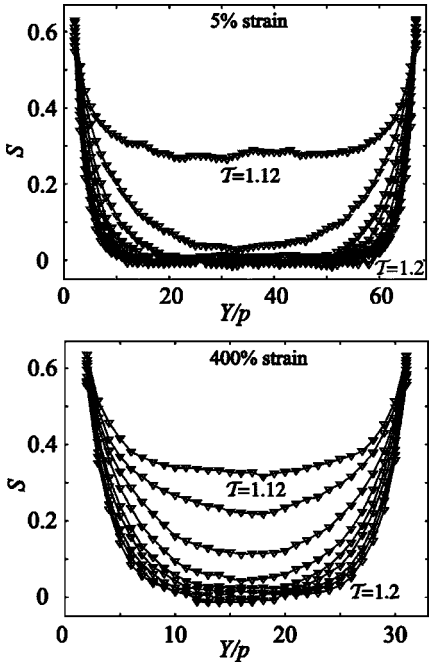

FIG. 13. Temperature scans of order parameter profiles plotted through the droplet center along the Y axis: (a) 5% strain, (b) 400% strain; temperature range $\mathcal{T}=1.12-1.20$ (curves top to bottom, step size 0.01). The subsurface degree of order S_0 shows no major temperature dependence and thus supports the temperature-independent model, Eq. (17).

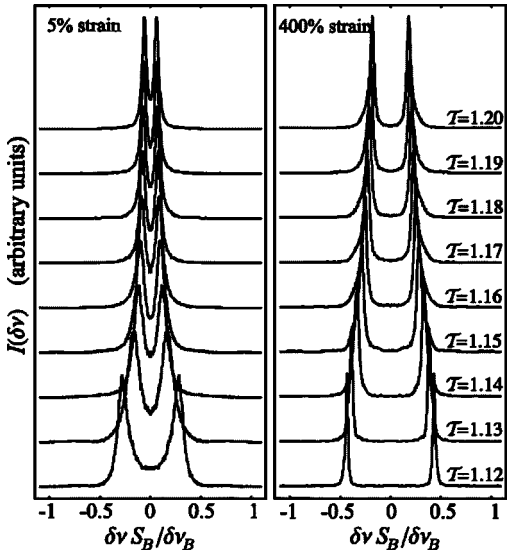

FIG. 14. Strained bipolar droplets: ^{2}H-NMR spectra; (a) 5% strain, (b) 400% strain. The quadrupole splitting decreases with temperature and increases with strain.

in the sample. The orientations $\mathbf{u}_j$ are obtained on the fly from the MC simulation, reproducing the effect of fluctuating molecular long axes. In addition, translational diffusion is simulated by an isotropic and homogeneous random walk process on the lattice [24].

The simulation box size was set to $70\times70\times70$ particles, allowing us to study droplets of size $68p$ in diameter. This already approaches 92 nm, the average droplet size in our experiment (see the above estimate for p). In case of strain the simulation box dimensions were adjusted according to Eq. (1) to roughly maintain the volume of the droplet (approximately 172 000 particles): $68\times68\times74$, $64\times64\times84$, $50\times50\times138$, and $32\times32\times342$ for 5%, 20%, 100%, and 400% strain, respectively. For each droplet geometry a separate temperature scan was performed, starting from a random configuration at $\mathcal{T}=k_BT/J=1.2$ and then simulating a gradual cooling down to $\mathcal{T}=1.12$ with a step of $\Delta\mathcal{T}=0.01$ (recall that the NI transition in the bulk LL model occurs at $\mathcal{T}_{NI}\approx1.1232$ [23]). At each temperature, 85×10^3 MC cycles were performed for equilibration, followed by 265×10^3 production cycles. During the acquisition of the FID signal, 1024 diffusion steps per NMR cycle were performed. This gives a root-mean-square molecular displacement of $32p$ per NMR cycle in the nematic phase [40] (and correspondingly more in the isotropic), which is already comparable to the unstrained droplet radius ($34p$) and thus approaches the fast diffusion limit. Like in the experiment, the spectrometer magnetic field was applied along the bipolar (tensile) axis—i.e., **b** parallel to X.

Figure 12(a) shows the director field for the droplet with 20% strain at $\mathcal{T}=1.20$. Bipolar paranematic ordering is well pronounced only in the vicinity of the substrate, with molecules on average aligned along the droplet symmetry axis, while in the bulk isotropic phase is restored. This surface-induced ordering is characterized by a nonzero nematic order parameter [see Fig. 12(b)] decaying to zero approximately exponentially, as assumed in Sec. V, with a characteristic length $\xi\sim4p$ on moving away from the substrate. This is also obvious from Fig. 13 showing nematic order parameter profiles for different temperatures, plotted along one of the

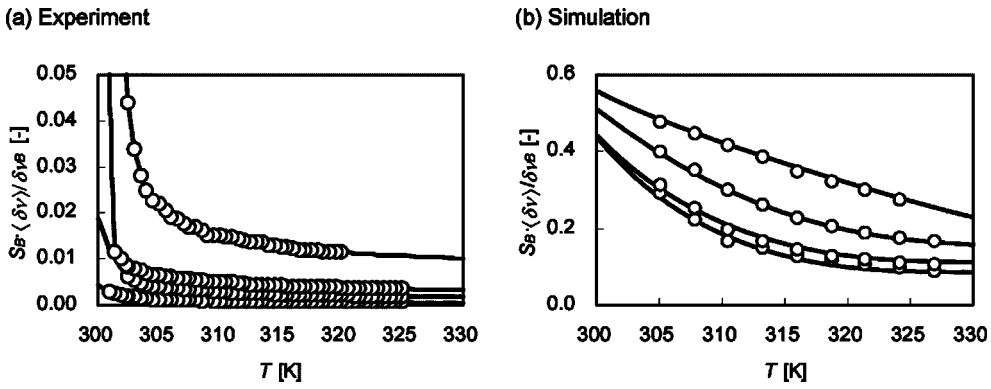

FIG. 15. Strained bipolar droplets: temperature dependence of the simulated quadrupolar splitting. Top to bottom: 400%, 100%, 20%, 5% strain. Experimental (*left*) vs simulated data (*right*). Bulk NI transition temperature for 5CB is ~302 K.

short principal axes of the droplet. One can clearly see the temperature dependence of the characteristic length ξ, while the subsurface value of the order parameter (S_0) exhibits a rather weak temperature dependence. The latter observation supports the use of the temperature-independent model for S_0 given by Eq. (17). There is, however, no major strain dependence for S_0 values since in the simulation the stretching process is only taken to affect the droplet shape, while only perfect (i.e., smooth) boundary conditions are considered. Note also that for strongly strained droplets (e.g., 400%) the length of the short droplet axis is substantially reduced, which leads to a capillary-condensation-like effect: due to the proximity of the opposing walls, nematic order is restored throughout the droplet even at temperatures several degrees above the bulk T_{NI} (Fig. 13).

Examples of the simulated ^{2}H-NMR spectra are shown in Fig. 14. Note that all spectra are double peaked, with no additional structure, which indicates that they are indeed highly diffusion averaged. The temperature dependences of the quadrupolar splitting for all droplets (estimated from the peak-to-peak distance for each spectrum) are summarized in Fig. 15. One can readily observe that the splitting decreases with increasing temperature and that it increases with strain, which are both seen also experimentally. The former effect is mainly because of the decrease of ξ—i.e., the thickness of the paranematically ordered subsurface layer—while the latter is due to a more pronounced orientation of nematic molecules along the tensile axis (and the spectrometer magnetic field), as well as due to an increase of the droplet surface area upon stretching the polymer matrix. Note, however, that all simulated values of the quadrupole splitting are noticeably higher than the experimental ones. This is a consequence of the rather strong coupling between nematic and ghost particles chosen in the simulation, resulting in an overestimate of the degree of paranematic order, including S_0. On the other hand, examining the increase of the quadrupole splitting upon stretching at a given temperature, one observes that at all temperatures the relative increase obtained experimentally is significantly larger than the corresponding MC-simulated value. Recall again that the simulations presented so far were performed with perfectly smooth bipolar boundary conditions at the droplet surface, while the actual appearance of the polymer substrate is far from smooth. Imperfections of the polymer surface lead to a decrease of the subsurface degree of ordering S_0 [40], which in a real system seems to be the case especially for weakly strained droplets trapped within a fairly disordered polymer. Then, with increasing strain, polymer chains disentangle, which is accompanied by an increase of S_0 (Fig. 11). In the simulated model systems we have shown, the increase of the quadrupolar splitting with stretching can be attributed solely to the change of droplet shape. In a real system this effect seems to be enhanced by the disentanglement process in the polymer matrix. For this reason, a set of simulations for partially disordered droplet surfaces has also been performed. A perturbation of bipolar boundary conditions was generated following a P_2-type orientational distribution with a controllable degree of surface order S_s [40]. This modification indeed

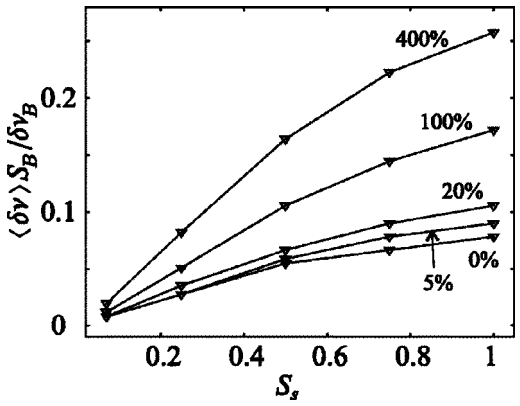

FIG. 16. Strained bipolar droplets: surface roughness dependence of the simulated quadrupolar splitting. Top to bottom: 400%, 100%, 20%, 5% strain, and no strain (for comparison only). On the abscissa the degree of surface-imposed order S_s is plotted. $\mathcal{T}=1.16$ ($\sim$312 K) in all cases.

reduces the quadrupole splitting, as can be easily concluded from Fig. 16. Extrapolating $S_s \rightarrow 0$ towards experimentally relevant values and using the experimental splitting data on stretching from 5% to 400% at $\mathcal{T}=1.16$ ($\approx$312 K), the simulation predicts an increase of S_s by a factor of $\sim$9. The experimental S_0 data from the fit, on the other hand, merely give a factor of $\sim$3.4. Note that in the low-S_s range the accuracy of curves plotted in Fig. 16 is limited as the magnitude of the resulting splitting already approaches the resolution of our spectra.

VII. CONCLUSION

In this paper, we have studied the alignment of 5CB-αd_2 in stretched PDLC's using ^{2}H-NMR. We have directly observed liquid-crystal alignment along the tensile axis in the nematic phase. Moreover, we have investigated paranematic surface-induced ordering and analyzed it using Landau–de Gennes theory. The elliptical model we propose is shown to well describe the surface ordering of liquid-crystal molecules confined to elliptical cavities. The measured surface value of the order parameter turns out to be largely temperature independent and is seen to increase with increasing strain. The latter observation is in agreement with the results obtained from optomechanical measurements [29]: on stretching, polymer chains of the PDLC matrix disentagle and thereby modify surface anchoring conditions for liquid-crystal molecules. Our experimental results are well correlated with qualitative trends obtained from Monte Carlo simulations of paranematic ordering in elliptical droplets.

ACKNOWLEDGMENTS

Financial support was provided by Fuji Photo Film Co. Ltd., the National Science Foundation (Grant Nos. DMR-0079964, DMR-9875427, and 0306851), and the Slovenian Office of Science (Programme No. P1-0099 and Slovene-U.S. Project No. SLO-US/04-05/32).

[1] P. Sheng, Phys. Rev. Lett. **37**, 1059 (1976); Phys. Rev. A **26**, 1610 (1982).
[2] T. J. Sluckin and A. Poniewierski, in *Fluid Interfacial Phenomena*, edited by C. A. Croxton (Wiley, New York, 1986), Chap. 5.
[3] G. P. Crawford, R. J. Ondris-Crawford, S. Žumer, and J. W. Doane, Phys. Rev. Lett. **70**, 1838 (1993).
[4] G. P. Crawford, R. J. Ondris-Crawford, J. W. Doane, and S. Žumer, Phys. Rev. E **53**, 3647 (1996).
[5] K. Miyano, Phys. Rev. Lett. **43**, 51 (1979); J. Chem. Phys. **71**, 4108 (1979).
[6] P. Guyot-Sionnest, H. Hsiung, and Y. R. Shen, Phys. Rev. Lett. **57**, 2963 (1986).
[7] R. Barberi and G. Durand, Phys. Rev. A **41**, 2207 (1990).
[8] W. Chen, L. J. Martinez-Miranda, H. Hsiung, and Y. R. Shen, Phys. Rev. Lett. **62**, 1860 (1989); T. Moses and Y. R. Shen, *ibid.* **67**, 2033 (1991).
[9] G. P. Crawford, D. K. Yang, S. Žumer, D. Finotello, and J. W. Doane, Phys. Rev. Lett. **66**, 723 (1991).
[10] G. P. Crawford, R. Stannarius, and J. W. Doane, Phys. Rev. A **44**, 2558 (1991).
[11] P. Ziherl, M. Vilfan, N. Vrbančič-Kopač, S. Žumer, R. J. Ondris-Crawford, and G. P. Crawford, Phys. Rev. E **61**, 2792 (2000).
[12] T. Jin, G. P. Crawford, R. J. Ondris-Crawford, S. Žumer, and D. Finotello, Phys. Rev. Lett. **90**, 015504 (2003)
[13] G. S. Iannacchione, G. P. Crawford, S. Žumer, J. W. Doane, and D. Finotello, Phys. Rev. Lett. **71**, 2595 (1993).
[14] G. S. Iannacchione, G. P. Crawford, S. Qian, J. W. Doane, D. Finotello, and S. Žumer, Phys. Rev. E **53**, 2402 (1996).
[15] G. S. Iannacchione, S. H. Qian, G. P. Crawford, S. S. Keast, M. E. Neubert, J. W. Doane, D. Finotello, L. M. Steele, P. E. Sokol, and S. Žumer, Mol. Cryst. Liq. Cryst. Sci. Technol., Sect. A **262**, 13 (1995).
[16] S. Kralj, G. Lahajnar, A. Zidanšek, N. Vrbančič-Kopač, M. Vilfan, R. Blinc, and M. Kosec, Phys. Rev. E **48**, 340 (1993).
[17] D. Finotello, H. Zeng, B. Zalar, and G. S. Iannacchione, Mol. Cryst. Liq. Cryst. Sci. Technol., Sect. A **358**, 237 (2001).
[18] B. Zalar, R. Blinc, S. Žumer, T. Jin, and D. Finotello, Phys. Rev. E **65**, 041703 (2002).
[19] G. P. Crawford and S. Žumer, *Liquid Crystals in Complex Geometries* (Taylor & Francis, London, 1996).
[20] A. Golemme, S. Žumer, D. W. Allender, and J. W. Doane, Phys. Rev. Lett. **61**, 2937 (1988).
[21] I. Vilfan, M. Vilfan, and S. Žumer, Phys. Rev. A **40**, 4724 (1989).
[22] M. Vilfan, N. Vrbančič-Kopač, B. Zalar, S. Žumer, and G. P. Crawford, Phys. Rev. E **59**, R4754 (1999).
[23] edited by P. Pasini and C. Zannoni, *Advances in the Computer Simulations of Liquid Crystals*, (Kluwer, Dordrecht, 2000).
[24] C. Chiccoli, P. Pasini, G. Skačej, C. Zannoni, and S. Žumer, Phys. Rev. E **60**, 4219 (1999); **62**, 3766 (2000).
[25] R. K. Bharadwaj, T. J. Bunning, and B. L. Farmer, Liq. Cryst. **27**, 591 (2000).
[26] I. Amimori, J. N. Eakin, G. P. Crawford, N. V. Priezjev, and R. A. Pelcovits (unpublished).
[27] P. S. Drzaic, *Liquid Crystal Dispersions* (World Scientific, Singapore, 1995).
[28] O. A. Aphonin, Yu. V. Panina, A. B. Pravdin, and D. A. Yakovlev, Liq. Cryst. **15**, 395 (1993).
[29] I. Amimori, N. V. Priezjev, R. A. Pelcovits, and G. P. Crawford, J. Appl. Phys. **93**, 3248 (2003).
[30] P. S. Drzaic, J. Appl. Phys. **60**, 2142 (1986).
[31] B. G. Wu, J. H. Erdmann, and J. W. Doane, Liq. Cryst. **5**, 1453 (1989).
[32] L. H. Sperling, *Introduction to Physical Polymer Science*, 2nd ed. (Wiley, New York, 1992).
[33] M. Vilfan, V. Rutar, S. Žumer, G. Lahajnar, R. Blinc, J. W. Doane, and A. Golemme, J. Chem. Phys. **89**, 597 (1988).
[34] G. P. Crawford, M. Vilfan, J. W. Doane, and I. Vilfan, Phys. Rev. A **43**, 835 (1991).
[35] A. Golemme, S. Žumer, J. W. Doane, and M. E. Neubert, Phys. Rev. A **37**, 559 (1988).
[36] P. G. de Gennes, *The Physics of Liquid Crystals* (Oxford University Press, London, 1974).
[37] P. G. de Gennes, Mol. Cryst. Liq. Cryst. **12**, 193 (1971).
[38] H. J. Coles, Mol. Cryst. Liq. Cryst. **49**, 67 (1978).
[39] P. A. Lebwohl and G. Lasher, Phys. Rev. A **6**, 426 (1972).
[40] C. Chiccoli, P. Pasini, G. Skačej, C. Zannoni, and S. Žumer, Phys. Rev. E **65**, 051703 (2002).